Published in final edited form as:
Hear Res. 2014 April ; 310: 1–12. doi:10.1016/j.heares.2014.01.003.

A subset of chicken statoacoustic ganglion neurites are repelled by Slit1 and Slit2

Andrea C. Battisti[1], **Kristen N. Fantetti**[1], **Bryan A. Moyers**, and **Donna M. Fekete**[*]
Department of Biological Sciences and Purdue University Center for Cancer Research, Purdue University, 915 W State St, West Lafayette IN 47907-1392, USA

Andrea C. Battisti: abattisti@medinst.com; Kristen N. Fantetti: kfantetti@gmail.com; Bryan A. Moyers: bamoyers@umich.edu; Donna M. Fekete: dfekete@purdue.edu

Abstract

Mechanosensory hair cells in the chicken inner ear are innervated by bipolar afferent neurons of the statoacoustic ganglion (SAG). During development, individual SAG neurons project their peripheral process to only one of eight distinct sensory organs. These neuronal subtypes may respond differently to guidance cues as they explore the periphery in search of their target. Previous gene expression data suggested that Slit repellants might channel SAG neurites into the sensory primordia, based on the presence of *robo* transcripts in the neurons and the confinement of *slit* transcripts to the flanks of the prosensory domains. This led to the prediction that excess Slit proteins would impede the outgrowth of SAG neurites. As predicted, axonal projections to the primordium of the anterior crista were reduced 2-3 days after electroporation of either *slit1* or *slit2* expression plasmids into the anterior pole of the otocyst on embryonic day 3 (E3). The posterior crista afferents, which normally grow through and adjacent to *slit* expression domains as they are navigating towards the posterior pole of the otocyst, did not show Slit responsiveness when similarly challenged by ectopic delivery of *slit* to their targets. The sensitivity to ectopic Slits shown by the anterior crista afferents was more the exception than the rule: responsiveness to Slits was not observed when the entire E4 SAG was challenged with Slits for 40 hours *in vitro*. The corona of neurites emanating from SAG explants was unaffected by the presence of purified human Slit1 and Slit2 in the culture medium. Reduced axon outgrowth from E8 olfactory bulbs cultured under similar conditions for 24 hours confirmed bioactivity of purified human Slits on chicken neurons. In summary, differential sensitivity to Slit repellents may influence the directional outgrowth of otic axons toward either the anterior or posterior otocyst.

Keywords

axon guidance; inner ear; neurite outgrowth; olfactory bulb; Slit; statoacoustic ganglion

1. Introduction

The vertebrate inner ear receives afferent innervation from bipolar neurons of the statoacoustic ganglion (SAG) that project a peripheral process to their sensory organ target

[*]Corresponding author. Tel.: +1 (765) 496-3058; Fax: +1 (765) 494-0876.
[1]These authors contributed equally to this manuscript.

and a central process into the hindbrain (Rubel and Fritzsch, 2002; Appler and Goodrich, 2011). These neurons originate from neuroblasts that delaminate from the floor of the otic cup and vesicle (Hemond and Morest, 1991). In the chicken embryo, delamination begins on embryonic day 2 (E2) and continues for several days, with the majority of neuroblasts generated by E4 (D'Amico-Martel, 1982; Hemond and Morest, 1991). The neuroblasts migrate into the mesenchyme, cluster into a cohesive group as the SAG and may continue to divide before differentiation commences. The earliest axons to emerge from the SAG project anteriorly and posteriorly towards the anlagen of the anterior and posterior cristae, respectively; these are the first organs to begin differentiation in the chicken (Wu and Oh, 1996). Over the next several days, as neuroblasts continue to delaminate, the tear-dropped-shaped otocyst develops into a complex membranous labyrinth that houses both auditory and vestibular organs.

Eventually, each peripheral axon will innervate only one of eight different sensory organs: anterior crista, lateral crista, posterior crista, utricular macula, saccular macula, macula neglecta, lagenar macula and the basilar papilla. Both attractive and repulsive cues may be active to correctly match each neuron with its appropriate target. Several highly conserved families of axon guidance molecules and their receptors are present during this pathfinding phase, including Ephs/ephrins (Siddiqui and Cramer, 2005), Semaphorins (Chilton and Guthrie, 2003), and Slits/Robos (Holmes and Niswander, 2001; Battisti and Fekete, 2008; Wang et al., 2013). Molecules that can influence otic axon outgrowth include neurotrophins (Tessarollo et al., 2004; Fritzsch et al., 2005), inflammatory cytokines (Bianchi et al., 2005; Banks et al., 2012), ephrins (Bianchi and Gray, 2002; Brors et al., 2003; Zhou et al., 2011; Coate et al., 2012), Semaphorins (Gu et al., 2003; Fantetti et al., 2011) and members of the BMP, Shh, and FGF morphogen families (Hossain et al., 1996; Hossain and Morest, 2000; Hossain et al., 2008; Fantetti and Fekete, 2012). Peripheral otic axon pathfinding has been the subject of recent reviews (Pauley et al., 2005; Webber and Raz, 2006; Fekete and Campero, 2007; Appler and Goodrich, 2011; Coate and Kelly, 2013).

During development, Slit ligands function as long- and short-range chemorepellents by signaling through Roundabout (Robo) transmembrane receptors. Slit-Robo signaling is classically known for regulating commissural axon guidance at the central nervous system midline (reviewed by Dickson and Gilestro, 2006; Reeber and Kaprielian, 2009), but is now known to also regulate neuronal and non-neuronal cell migration, cell polarity, axon targeting, and axon guidance in several other neural systems (reviewed by Ypsilanti et al., 2010). Currently, two Robo homologues and three Slit homologues have been identified in the chick (Bashaw and Goodman, 1999; Li et al., 1999; Vargesson et al., 2001).

Expression data for the developing chicken inner ear suggest that Slits and Robos could be involved in several different aspects of otic patterning and axon guidance (Battisti and Fekete, 2008). *Slit -1, -2* and *-3* transcripts were detected within the otocyst adjacent to the forming SAG. Also, localized expression of *robo* transcripts in both the neurogenic domain of the otocyst and within the SAG led us to speculate that neuroblasts are probably Slit responsive and that Slit-mediated repulsion might promote neuroblast delamination. However, neuroblast delamination is normal in Slit2 and Robo1/2 mutant mice, although at a later stage spiral ganglion cohesion and spatial positioning were disrupted in the cochlea (Wang et al., 2013). We also proposed that the earliest afferents projecting towards either the anterior or posterior crista might be repelled from entering territories where Slits are expressed, thereby channeling them toward their appropriate targets. Finally, we suggested that Slits might be involved in the establishment or maintenance of sensory/nonsensory boundaries because these adjacent territories express Slits (non-sensory) and *robo1/2* (prosensory).

In this study, we used *in ovo* gain-of-function to ask whether Slit-Robo signaling might influence the formation of the SAG, channeling of neurites towards the anterior and posterior cristae, or the integrity of the prosensory patches. In addition, to test the hypothesis that SAG axons are repelled by Slits, isolated SAG explants were challenged with purified Slit proteins and then assayed for evidence that neurite outgrowth was inhibited. Our results show that most otic axons are not repelled by either Slit. One exception is the population of afferents projecting to the anterior crista; this group fails to enter its target if either *slit1* or *slit2* is ectopically expressed there. In contrast, posterior crista afferents are unimpeded when *slits* are introduced into their target. These data indicate that the myriad of sensory afferents projecting to different prosensory targets may have intrinsic differences in the guidance molecules that they use while pathfinding. Also, forced expression of *slits* does not alter SAG formation or the establishment of prosensory domains in the inner ear.

2. Materials and methods

2.1 Plasmids

A previous study inserted full-length coding sequences for human SLIT1 and SLIT2 into the pcDNA3.1/his-myc vector to encode bioactive proteins tagged with the myc epitope on their C-termini under the control of a cytomegalovirus (CMV) promoter (Patel et al., 2001). The myc-tagged proteins were purified from the supernatant of transfected cells by immunoprecipitation and Western blotted to show that ~200kD full-length hSLIT1-myc and hSLIT2-myc were secreted, as well as a 55-60kD cleavage fragment of hSLIT2 (Patel et al., 2001). For the experiments reported here, each gene was retained in its original plasmid backbone, but the CMV promoter was replaced with the EF1a promoter as follows. The pEF1-Slit1 and pEF1-Slit2 plasmids were constructed by replacing the CMV promoter in the original CMV-Slit:myc constructs with the EF-1α promoter derived from pEFX. The pEFX-GFP construct contains GFP under the control of an EF-1α (elongation factor 1 alpha) promoter (Agarwala et al., 2001). pEFX was generated by modifying pEF1/myc-His (version C, Invitrogen) such that a 2.2kb fragment between the PvuII sites, containing neomycin and SV40 elements, was excised. The resulting pEF1-Slit1 and pEF1-Slit2 constructs are 10.7kb and 10.1kb, respectively. These two plasmids were used for transfection of HEK cells (ATCC) and for electroporations into the chicken otocyst. For some experiments, Slit expression plasmids were co-electroporated with pEFX-GFP (3:1 molar ratio of pSlit:pEFX-GFP).

2.2 Electroporation into the otocyst

Eggs were windowed on E2 and staged according to Hamburger and Hamilton (Hamburger and Hamilton, 1951). Chick Ringer's solution (7.2 g/L NaCl, 0.23 g/L CaCl, 0.37 g/L KCl, 0.115 g/L Na_2HPO_4, pH 7.4) was dripped onto the amnionic sac to facilitate opening it to expose the right otocyst. Plasmid DNA (4-8 μg/μl) was microinjected into the right otic cup/vesicle of HH15-18 embryos with pulled glass micropipettes (10-12 μm diameter) using a picospritzer. A pair of homemade platinum paddle-shaped electrodes was positioned adjacent to the anterior and posterior sides of the otocyst. Electrodes were constructed using insulated tubing (heat shrink 3/64" BK 6", SPC Technology) to shrink-wrap a small piece of platinum wire (0.01", World Precision Instruments) to a longer piece of tungsten wire (0.02", Alfa Aesar), such that only the platinum tip was exposed. Nail polish was used to coat the outside edges of the platinum paddles to direct the current between the two electrodes. Two or three 10-volt square wave pulses, each 50 milliseconds long and spaced 10 milliseconds apart, were administered using a TSS20 Ovodyne electroporator connected to an EP21 Current Amplifier (Intracel, UK) following modified protocols (Momose et al., 1999; Krull, 2004). The cathode was connected to the electrode in front of the otocyst to target the anterior crista or behind the otocyst to target the posterior crista. Ringer's solution

was dripped onto the electrodes before they were removed. The conducting surface of each electrode was cleaned with a damp Kimwipe after each embryo. Embryos were returned to the 37°C incubator and sac rificed 24-72 hours later at HH21-28 (anterior crista) and HH23-28 (posterior crista).

2.3 Histological analysis of electroporated tissue

Heads were fixed in 4% paraformaldehyde in phosphate-buffered saline (PBS), dehydrated in 15% sucrose and frozen in Tissue Freezing Media (Triangle Biomedical Sciences). Transverse or horizontal sections of 15 μm thickness were collected onto Superfrost Plus slides (Fisher Scientific). Axonal processes were labeled with one of three different antibodies: NF70 (rabbit polyclonal raised against gel-purified chicken 70kD neurofilament protein, 1:200, provided by Dr. Peter Hollenbeck, Purdue University); 3A10 (mouse monoclonal IgG_1 raised against chicken neural tube and associated with neuroflaments, 1:50 of hybridoma cell culture supernatant, Developmental Studies Hybridoma Bank; DSHB); or TuJ1 (mouse monoclonal IgG_{2a} directed against β-tubulin III, 1:2000, Sigma). If pEFX-GFP was included in the transfection, the protein's natural fluorescence was enhanced in the green channel by immunostaining all sections with anti-GFP anti-rabbit polyclonal antibody (1:1000, Invitrogen) and AlexaFluor488-conjugated secondary antibodies. For pEFX-GFP electroporation with or without pSlit co-electroporation, sequential sections were immunostained with 3A10, TuJ1 or anti-Sox2 (goat polyclonal Y-17, 1:250, SantaCruz Biotechnology) and processed for detection in the red channel with AlexaFluor588 secondary antibodies. For embryos electroporated with Slit plasmids only, one series was co-labeled with NF70 and an anti-myc mouse monoclonal antibody (9E10, IgG_1 undiluted cell culture supernatant from hybridoma cells; DSHB) and alternate sections were labeled with anti-Sox2. Secondary antibodies conjugated to AlexaFluor dyes (1:500, Invitrogen) were used to detect primary antibodies as follows: 568 goat anti-rabbit IgG (NF70); 568 goat anti-mouse IgG_1 (3A10); 568 goat anti-mouse IgG_{2a} (TuJ1); 568 donkey anti-goat IgG (Sox 2); 488 goat anti-mouse IgG_1 (myc); and 488 donkey anti-rabbit IgG (GFP). After immunostaining, sections were coverslipped with VectaShield HardSet (Vector Laboratories). Qualitative assessments of sensory innervation patterns were conducted with a 20x objective on a Nikon Eclipse E800 fluorescent microscope. For basic histology, frozen sections were rinsed with PBS between sequential incubations with 3A10 antibody, biotinylated horse anti-mouse IgG (1:250; Vector Laboratories), and ABC reagent (avidin-biotin-horseradish peroxidase; Vector Laboratories). Following diaminobenzidine histochemistry, the slides were counterstained with cresyl violet.

2.4 Quantification of innervation, sensory organ size, and SAG size *in vivo*

A subset of electroporated specimens was used for quantitative analysis of axonal innervation and the sizes of the SAGs and sensory cristae. Immunostained cryosections were imaged with a 20x objective on a Nikon C1-plus confocal microscope. Maximal intensity projections were created and measurements were performed using NIH ImageJ software. NF70-positive pixels were summed to quantify sensory organ innervation as previously described (Fantetti et al., 2011). Briefly, alternate images containing NF70-positive axons were converted to black (neurites) and white (background). The innervated region was encircled, the image was cropped, and the number of black pixels was counted. Sensory organ size or SAG size (area in μm^2) was measured by outlining either the Sox2-positive anterior/posterior crista or the defined edge of the SAG, respectively. The number of black pixels (neurites) per sensory organ, sensory organ size and SAG size was obtained for each section and then summed across the entire organ (typically 4-7 sections). Values for the right ear (electroporated) were normalized to the left ear (unelectroporated control). These ratios were calculated for the pEFX-GFP (control) and pEF1-Slit1-electroporated embryos and presented as mean ± standard error (SE).

2.5 Statistical analysis of electroporated embryos

Electroporated embryos were pooled across multiple experiments to obtain sufficient numbers for statistical comparisons. Although 10-20 embryos were usually electroporated on the same day, relatively few embryos from each batch were included in the quantitative analyses because each had to meet specific selection criteria including survival, successful electroporation of the targeted sensory organ, high quality sectioning and immunostaining, and normal inner ear morphogenesis (see Results section for further details). Each animal served as its own control by comparing left and right ears to account for variations across egg batches such as incubation conditions or differences in measured parameters based on developmental age.

Each embryo with a correctly targeted sensory organ was evaluated qualitatively as having normal or reduced innervation into the electroporated organ as compared to the same organ on the contralateral side. These data are presented in Table 1 and were evaluated for statistical significance using a Fisher's exact test.

Quantitative measurements of electroporated embryos were subjected to additional statistical analysis to query the data for potential batch-related variation. We used a linear mixed model where the response variable was the ratio (right ear/left ear) for a specimen and the factors are treatment (GFP vs. Slit1) and batch (experiments run on the same day). We also allowed the specimen-to-specimen variability to be different across the two treatments and required all variance estimates to be greater than or equal to zero. A Keward-Rogers denominator degrees of freedom (df) approximation method was used to calculate the appropriate df for the treatment comparison. We report the mean estimates and their SE, along with the df and p-value for the treatment comparison. Results suggest relatively little batch to batch variability so the test results are comparable to ignoring batch and performing a two-sample t-test.

2.6 Explant dissection and culture

White Leghorn chicken eggs (Purdue University Farm) were incubated at 37°C, removed from the egg, assigned HH stages according to Hamburger and Hamilton (1951), placed into chick Ringer's solution and quickly decapitated. Fine dissections were performed in Hank's Balanced Salt Solution (HBSS; Sigma). Olfactory bulbs were removed from embryonic day 8 (E8) embryos (HH32-34) and SAGs from E4 embryos (HH20-25). SAG and olfactory bulb explants were cultured in 1.5 mg/ml rat-tail type I collagen (BD Biosciences), as described (Bianchi and Cohan, 1993; Fantetti et al., 2011; Fantetti and Fekete, 2011; Fantetti and Fekete, 2012), in serum-free medium supplemented with 10 ng/ml Neurotrophin-3 (NT3; Sigma) and 10 ng/ml Ciliary Neurotrophic Factor (CNTF; Sigma). Experimental groups were cultured in medium supplemented with recombinant mouse Slit1 and/or mouse Slit2 diluted in PBS to 0.5, 1, 5, 10 or 20 μg/ml. The manufacturer (R&D Systems) recommends using the Slit proteins at 3-12 μg/ml, based on the enhanced neurite outgrowth of dissociated E13 chick dorsal root ganglion neurons. PBS was added to control cultures. Olfactory bulb and SAG explants were cultured for 20h and 40h, respectively, under serum-free conditions. Cultures were fixed and immunostained with monoclonal anti-β-tubulin (Sigma), as described (Fantetti and Fekete, 2011; Fantetti and Fekete, 2012).

2.7 Quantification of neurite outgrowth *in vitro*

Confocal images of SAG and olfactory bulb cultures were captured on a Nikon EFD-3 microscope using a BioRad MRC-1024 laser. Measurements were performed on maximum intensity projection images generated from confocal z-stacks. To quantify the area occupied by outgrowing neurites, pixel measurements were performed as described (Fantetti et al., 2011). Briefly, image projections were converted to black (neurites) and white (background)

and each image was divided into 4 quadrants. The number of black pixels was normalized to a smooth arc drawn along the perimeter of the measured quadrant (referred to as explant length), as a control for explant size. To measure neurite outgrowth from the same quadrant, the length of each neurite bundle was measured from the perimeter of the explant to the distal-most tip of the bundle. The average length of approximately 30-50 bundles was calculated for each explant. Bundle length and pixel numbers are presented as mean ± SE. To compare average measurements between controls and treated samples, we used a multi-way ANOVA with treatments and blocks (separate experiments) as independent variables, followed by multi-test correction using the Benjimin-Hochberg Method.

3. Results

3.1 Human SLIT1 and SLIT2 electroporation constructs

The expression constructs used for *in vitro* and *in vivo* experiments encode C-terminal myc-tagged human *SLIT1* and *SLIT2* genes. These genes are bioactive in the chicken hindbrain when driven with a CMV promoter (Hammond et al., 2005). Our initial results showed poor *in vivo* expression of the Slit-myc fusion proteins following electroporation into the otic vesicle (data not shown), even though nearly 100% of HEK cells transfected with the same plasmids were myc-positive (not shown). Our concern was that the CMV promoter was not optimal for otic epithelial expression, which led us to try the EF1-α promoter instead; we found this promoter to be highly effective at transducing GFP into the otic epithelium. Thus, myc-tagged *SLIT1* and *SLIT2* were subcloned into pEF1 vectors and were used for otic vesicle electroporations. While this led to modestly improved myc detection in Slit1-electroporated inner ears, the signal was still far below that observed by immunostaining for GFP when pEFX-GFP was cotransfected. Subsequently, we determined that the CMV promoter did effectively drive expression of a relatively small myc-tagged protein, Jun Dimerization Protein 1 (not shown) in the otic epithelium. Therefore, the apparent difficulty of detecting robust Slit expression with CMV drivers may be unrelated to the promoter and instead may reflect the larger size of the *SLIT* plasmids (~10kb) as compared to the GFP plasmid (~4kb). It is also possible that the myc epitope was not readily accessible for immunodetection in inner ear tissue sections.

3.2 Misexpression of Slit1 reduces innervation to the prosensory domain of the anterior crista but not the posterior crista

This study used the ectopic delivery of Slit expression plasmids into the prosensory cristae to test SAG neurites for Slit responsiveness. Specifically, we predicted that responsive neurites would fail to penetrate the sensory epithelium if Slit proteins were present when the afferents arrive at their target. The primordia of the anterior and posterior cristae can be readily electroporated with plasmids at HH15-18 by placing electrodes at the anterior and posterior poles of the otocyst (Chang et al., 2008). At HH19, the earliest axons make contact with the incipient anterior crista (Hemond and Morest, 1991). Immunostaining with a neurofilament antibody shows axons reaching the posterior crista a few hours later (HH22; data not shown). Horizontal sections through the chick heads 2-3 days after transfection offer views of vertical canal pouch formation as an indicator of the morphogenetic progression of the dorsal ear (Fig. 1A) and show axon bundles emerging from the SAG to innervate crista primordia at the anterior (Fig. 1B) and posterior (Fig. 1C) poles of the otocyst.

Electroporation parameters were optimized using a control GFP construct (pEFX-GFP) to obtain maximal transfection of the otic epithelium with minimal disruption of development (Fig. 2A-H). We evaluated whether innervation of the anterior crista primordia was similar in electroporated (right) and non-electroporated (left) ears within the same embryo, and

harvested at various time points at HH21-28. Strong GFP expression was visible in ~75% of the cells at the anterior pole of electroporated ears (Fig. 2E). A monoclonal antibody raised against chicken axons (NF70) was used to visualize the presence of nerve fibers that reached or entered the anterior prosensory region. We defined innervation as axons touching or entering the sensory primordium. When the anterior crista and/or adjacent epithelium were transfected with pEFX-GFP, innervation in the electroporated ear (Fig. 2F) was comparable to the control, non-electroporated ear (Fig. 2B) in 20/23 of the specimens examined. This confirmed that the electroporation procedure itself rarely altered axonal projections to the anterior crista.

The observed reduction of innervation to the anterior crista in a small subset of the GFP-electroporated ears (3/23) was likely an electroporation-induced artifact. Indeed, a subset of otocysts appeared smaller on the electroporated sides when harvested on E5 or E6 (not shown). This included ears that were transfected with either pEFX-GFP alone, Slit plasmids alone, or a combination. When processed on E6 (HH27-28), the smaller ears were found to have defects only in their dorsal halves. Specifically, the walls of the vertical pouch on the experimental side were further apart than those on the contralateral control side, which by comparison were flattened in the medial-lateral dimension as though preparing for canal plate fusion (see Fig. 1A). Also, when the vertical pouch appeared inflated on the electroporated side, it was also smaller than the control side both in its anterior-posterior dimension and in its dorsal-ventral dimension. Notably, the ventral half the inner ear appeared normal in all cases. A subset of Slit-electroporated ears with the most severe dysmorphogenesis in the vertical pouch had an anterior crista that was either absent entirely or was not obviously separated from a continguous Sox2-positive patch that contained the primordia of the lateral crista and the utricular macula. In others, the anterior and posterior cristae were identifiable as separate Sox2-positive domains, but were obviously smaller than the control side. Not surprisingly, smaller cristae always had reduced innervation in comparison to the contralateral sides. In some experimental batches, dysmorphogenesis was evident for nearly half of the Slit-electroporated ears, which were typically more severely affected than GFP-electroporated control ears from the same batch. Because small or absent cristae were always associated with small vertical pouches, all specimens with dorsal ear dysmorphogenesis and/or noticeable reduction in the size of the cristae were excluded from subsequent analyses. This allowed us to focus on the question of whether the peripheral processes of crista afferents are responsive to Slits.

Results from Slit1-myc electroporations were analyzed quantitatively and are described first. An antibody directed against the myc epitope was used to identify cells that were transfected with the Slit1 plasmid. Slit1-myc expression was consistently weaker than GFP expression in comparisons across embryos (compare Fig. 2E and 2M). Innervation of the prosensory anterior crista was compared between Slit1-electroporated (right) and non-electroporated (left) ears. The majority (18/22 ears) showed either reduced or complete loss of innervation to the anterior prosensory patch on the Slit1-transfected side (Fig. 2N), compared to controls (Fig. 2J). This stands in marked contrast to the number of GFP-transfected anterior crista showing reduced innervation (3/26). This difference, summarized in Table 1, was statistically significant (Fisher's Exact test, $p<0.0001$). The observed reduction in anterior crista innervation was statistically significant in a subset of ears that were quantitatively analyzed (Fig. 2Q; $df = 6.88$, $p<0.0001$).

The severity of the phenotype was associated with how robust and diffuse Slit1-myc expression was within the anterior crista epithelium. In cases of weak Slit1-myc expression and reduced innervation, a small number of axons appeared to touch the sensory epithelium containing Slit1-transfected cells, but did not enter the epithelium (not shown). Additionally, in cases where a small number of afferents contacted the prosensory region, some axons

appeared more tightly fasciculated than controls that instead spread more uniformly across the prosensory patch (not shown). It is possible that some axons reached their anterior target before the Slit protein was expressed at levels sufficient for bioactivity. Alternatively, a subset of the afferent axons may be insensitive to Slit1 and are thus able to enter the anterior crista despite the presence of Slit1-misexpressing cells. Following Slit1-misexpression, reduced innervation of the anterior crista was visible at the earliest stage examined (HH21) and persisted through the latest stage examined (HH28). The same result was obtained when axons were detected with either the NF70 antibody to detect the low-molecular weight neurofilament protein or the 3A10 monoclonal antibody to detect a neurofilament-associated epitope (not shown).

When the posterior crista primordium was targeted with pEFX-GFP, innervation appeared normal in all cases (Fig. 3A-F, n=16) at HH23-27. Similarly, following pEF1-Slit1 electroporation into the posterior crista (Fig. 3J), innervation of the posterior prosensory patch was similar between left and right ears (Fig. 3H, K; n=20). Quantitatively there was no significant difference in posterior crista innervation between electroporated and non-electroporated ears (Fig. 3M; df=8.66, p=0.1082). These results suggest that in contrast to anterior crista afferents, posterior crista afferents are insensitive to Slit1 *in vivo*. Results are summarized in Table 1.

3.3 Prosensory formation is unaffected in Slit1-electroporated ears with a normal sized vertical pouch

We considered whether the paucity of innervation observed in experimental ears was confounded by electroporation-induced developmental defects in the anterior crista, rather than to the misexpression of Slit1, even in ears with normal canal morphogenesis. To address this, the size and position of the prosensory cristae were evaluated using antibodies against Sox2 (Stone et al., 2003; Neves et al., 2007). The development of the anterior (Fig. 2C, G, K, O) and posterior (Fig. 3C, F, I, L) cristae primordia in pEFX-GFP- and pEF1-Slit1-electroporated ears were compared to those on the contralateral, non-electroporated side in ears showing a vertical canal pouch of normal size and morphology. Sox2 immunostaining revealed that both cristae were comparable in location and size on left and right sides (Anterior: Fig. 2R; df=3.97, p=0.3803, Posterior: Fig. 3N; df=5.06, p=0.4401). These results suggest that the paucity of innervation following Slit1 transfection was unlikely to be caused by defective prosensory specification in those ears.

3.4 Slit1 misexpression in the anterior otocyst did not affect SAG formation

In the present study, all embryos were electroporated between HH15 and18, which coincides with peak neuroblast delamination and SAG formation (Hemond and Morest, 1991). At this time, transcripts for both *slits* and *robos* are weakly expressed within the otic epithelium and neuroblasts show strong *robo2* expression. This suggests that neuroblasts may be Slit-responsive during stages of migration and SAG formation (Battisti et al., 2008). When the plasmids were targeted to the anterior pole, most pEFX-GFP- and/or pEF1-Slit1-electroporated embryos contained GFP-positive or myc-positive SAG neurons (insets in Fig. 2H, P), indicating that the neurogenic region of the otocyst was targeted during delamination and/or that the ganglion itself had been transfected during gangliogenesis. This raised the question of whether reduced anterior crista innervation was an indirect effect of the electroporation itself or the misexpression of Slit1 in the ganglion, either of which might reduce the pool of SAG neurons or disrupt gangliogenesis. We examined SAG size to evaluate these possibilities.

Studies from chick and zebrafish systems suggest that disrupting SAG formation would result in a change in SAG size, measured after HH21 in the chick (Hossain et al., 1996;

Camarero et al., 2003; Adamska et al., 2001). Two days after transfection, SAG size was compared between left and right ears within the same embryo, for pEFX-GFP- and pEF1-Slit1- electroporated embryos. Qualitatively, the position and shape of the SAG was similar for left and right ears in both treatment groups (Fig. 2D, H, L, P). Quantitatively, there was no significant difference in SAG size between electroporated and unelectroporated ears (Fig. 2S; df=6.51, p=0.7202). These results suggest that the reduction in anterior crista innervation is not due to a major disruption in SAG formation, although a quantitative analysis of neuron numbers would be needed to determine whether a small subset of SAG neurons might be missing in response to Slit overexpression.

3.5 Misexpression of Slit2

An initial set of pEF1-Slit2 electroporated ears (n=15) showed either none or only a few myc-transfected cells, even in the subset of cases where co-transfection with pEFX-GFP revealed that the anterior and posterior poles of the otocyst were successfully electroporated and GFP-expressing (n=6/8). An additional pEF1-Slit2 plasmid prep was prepared at 2-fold higher concentration (9.3 μg/ml vs. 4.5 μg/ml) and used in a series of subsequent experiments. Again, myc immunolabeling was rarely detected in the transfected ears. Thus, for subsequent Slit2 experiments, pEFX-GFP was co-transfected with pEF1-Slit2 so that GFP immunofluorescence could be used to identify targeted cells. When GFP-positive cells were present within the Sox2-positive anterior crista domain of ears with normal vertical pouch morphogenesis, the number of axons traveling to the anterior crista and penetrating the sensory epithelium was drastically curtailed in the majority of specimens (n=6/7) (Fig. 4). In contrast, when Slit2/GFP co-electroporations were successfully targeted to the posterior crista, innervation appeared robust in morphologically normal ears (n=6; data not shown). These data are statistically significant only for the anterior crista (Fisher's Exact test, $p<0.0001$). Although not deliberately targeted, GFP was occasionally detected in other sensory primordia following Slit2/GFP co-electroporations. This includes the lateral crista, the utricular macula and the saccular macula. The density of axons projecting to these transfected organs was qualitatively indistinguishable from the contralateral ears.

It was important to verify that the apparent reduction of anterior crista afferents was indeed due to a failure of axons to reach or penetrate the epithelium, and not due to an absence of neurofilaments or their associated proteins. To address this, we used a TuJ1 monoclonal antibody to label class III β-tubulin. Individual sections through the inner ears of a HH25 untransfected embryo were double-labeled for both TuJ1 and NF70. The two antigens showed nearly complete overlap in the labeling of axon bundles and individual processes entering inner ear sensory primordia (data not shown), although TuJ1 also weakly labeled most otic epithelial cells, while both NF70 and 3A10 did not. In ears co-transfected with Slit2 and GFP plasmids, the green channel was used for GFP detection and the red channel for detection of axons immunolabeled with either 3A10 or TuJ1 on alternate sections, to determine if both epitopes revealed comparable innervation deficits when plasmids were targeted to the anterior crista. Indeed this appears to be the case. Figure 4 shows sections through an untransfected left ear (Fig. 4A) and a right ear with the anterior cristae well-targeted by electroporation, based on GFP immunofluorescence (Fig. 4E). Both TuJ1 and 3A10 antibodies detected a similar number and arrangement axons in alternate sections through the cristae of the contralateral control ear that has robust innervation (Fig. 4B and 4C). Similarly, on the electroporated side, the two antigens are also concordant. Specifically, both reveal the presence of two small bundles of axons that approach the anterior crista and each bundle projects only a few axons into the epithelium (Fig. 4F and 4G). A normal-sized crista primordium was identified on each side by expression of Sox2 (Fig. 4D and 4H). The observation that TuJ1 and 3A10 immunostaining patterns were similar on adjacent sections was confirmed for a total of 12 embryos (4 Slit2/GFP, 5 Slit1/GFP and 3 GFP).

3.6 The majority of otic neurites are not repelled by Slit1 and Slit2 in vitro

We wished to evaluate whether or not the majority of otic axons would be Slit-responsive, but it proved difficult to target each of the prosensory anlagen by electroporation. As an alternative, we used an *in vitro* system that had previously demonstrated that SAG neurite outgrowth is reduced by Semaphorin 3E (Fantetti et al., 2001) and enhanced by secreted ligands such as BMPs and FGFs (Fantetti and Fekete, 2012). As described below, we were unable to reproduce the *in vivo* response to Slits using this *in vitro* assay.

Prior to initiating Slit assays on cultured SAGs, positive control experiments were conducted on E8 chick olfactory bulb explants (Li et al., 1999). These cultures were used to confirm the bioactivity of purified mouse Slit proteins on chicken neurons. Olfactory bulbs were cultured in the presence of 0-20 μg/ml Slit1 or Slit2 for 20 hours. A dose of 20 μg/ml of Slit1 or Slit2 significantly reduced the mean pixels/explant length compared to control medium with PBS additive (Fig. 5A-C). At 10 μg/ml, only the Slit2 treatment reached a statistically significant reduction ($p<0.0001$ ANOVA, data not shown).

A dose-response curve was then conducted by culturing SAGs in the presence of Slit1 or Slit2 at 0, 0.5, 1, 5 or 20 μg/ml. Ganglia were processed after 40 hours and outgrowth was comparatively robust in all conditions. No statistically significant differences were detected in either neurite length (ANOVA; Slit1, $p=0.8403$; Slit2, $p=0.6803$) or pixels/explant length (Slit1 $p=0.5058$; Slit2, $p=0.3118$) between the treatment groups. Below we present results for SAG explants incubated with the highest dose (20 μg/ml) of each Slit, either alone or in combination.

E4 SAG cultures treated purified Slit proteins for 40 hours showed no qualitative difference between treatment groups in the robustness of the outgrowth corona (Fig. 5D-G). Quantitatively, there was no significant difference in the average length of neurite bundles (Fig. 5H; ANOVA, $p=0.1742$) or average pixel number (Fig. 5I; ANOVA, $p=0.9500$), between control and Slit-treated SAG explants. Since bioactivity of the Slit proteins was confirmed (Fig. 5A-C), these results suggested that the large majority of SAG neurites were unresponsive to purified Slits at the doses tested.

3.7 SAG neurite unresponsiveness to Slit1 and Slit2 is not age-dependent

We next interrogated the explant data for whether Slit responsiveness might vary depending upon the age of the embryo when the ganglion was explanted. The timing of afferent and efferent outgrowth and innervation of the sensory epithelium is well characterized. Vestibular axons invade the sensory epithelia on E4 at HH24 (Ginzberg and Gilula, 1980) while the auditory axons invade the basilar papilla on E6 at HH29 (Whitehead and Morest, 1985). Prior to HH24, outgrowth from the SAG most likely represents pioneer vestibular axons, whereas outgrowth from HH24 onwards likely consists of later-emerging vestibular axons along with auditory axons. By extrapolation, data from these studies suggest that the composition of axons extending from the E4 SAG *in vitro* might also differ with stage of the embryo at the time the ganglion was removed. Therefore, we separately analyzed SAGs from younger embryos (HH20-23; n= 6 ganglia per condition) versus older embryos (HH24-25; n= 6 ganglia per condition except Slit1+2 n=5 ganglia). No differences were observed between Slit treatment groups and controls in either age subpopulation for average neurite length (ANOVA, HH 20-23, $p=0.6280$; HH24-25, $p=0.7878$) or average pixels/length (ANOVA, HH 20-23, $p=0.6980$; HH 24-25, $p=0.6980$).

4. Discussion

4.1 Anterior crista afferents are repelled by Slits *in vivo*

The earliest axons to emerge from the chicken SAG project towards the anterior crista, followed by those projecting towards the posterior crista. Upon their arrival at these two targets, the afferents are not expected to encounter Slits within the sensory primordium, based on a survey of their transcript expression (Battisti and Fekete, 2008). We took advantage of this fact to test the responsiveness of crista afferents to Slits by overexpressing them within their targets so that excess Slit proteins would be present approximately at the time the afferents arrive. Slit-mediated repulsion should manifest as a reduction or absence of afferent innervation in the presence of ectopic Slit expression. Indeed, fewer axons innervated the anterior crista primordium when Slit1 or Slit2 was misexpressed in the anterior prosensory patch. Why might these axons be sensitive to Slits in the normal ear? Axons emerge from the SAG by HH17 (Kuratani et al., 1988) and first contact the anterior crista on HH19 (Hemond and Morest, 1991). During this time window (HH17-19), *in situ* hybridization data show strong expression of *robo2* in the SAG, so evidence of Slit responsiveness was to be expected. The localization of *slit1* transcripts within the posterior third of the SAG by HH15/16 and *slit2* by HH23 may explain why anteriorly-directed axons are Slit-responsive. Assuming that the presence of these transcripts reflects a localized source of secreted Slits, then Robo-expressing neurons attempting to travel through this region would be repelled. That is, a source of Slits may be positioned here to redirect misguided anterior crista afferents back toward the direction of their correct target. This is shown schematically in the model of Fig. 6 as a white cell body with a posteriorly-misdirected neurite that fails to advance in the posterior direction.

4.2 Posterior crista afferents are not repelled by Slits *in vivo*

In contrast to the results of Slit overexpression in the anterior crista primordium, similar repulsion was not observed when Slits were targeted to the posterior crista primordium. A possible explanation for their apparent lack of responsiveness to Slits is that afferents projecting toward the posterior pole of the otocyst may normally encounter Slit proteins en route, including within the SAG itself as described above. If these growing neurites were repelled by Slits during their navigation, they might not succeed in emerging from the ganglion, or they might be misdirected anteriorly. On the other hand, we had predicted that posterior crista afferents might require Slit-responsiveness after they emerge from the ganglion and begin to navigate posteriorly. The idea was based on the detection of *Slit* transcripts within the medial otic epithelium (shown as dashes in Fig. 6), immediately adjacent to where the posterior crista afferents were projecting on their way to the posterior pole (Battisti and Fekete, 2008). We considered that Slit-mediated repulsion might prevent the neurites from terminating prematurely in a region that could otherwise be attractive, since this epithelium eventually differentiates as the saccular macula. Such a repulsive activity could ensure that at least some axons project all the way to the posterior pole of the otocyst. However, this study failed to demonstrate the predicted repulsive effect of Slits on posterior crista afferents between the time of transfection (HH15-18) and the stages examined (HH23-28). Since afferents traveling to the posterior crista are reported to arrive at this prosensory patch by HH24 (Von Bartheld et al., 1991), we expected to see reduced innervation if these axons are indeed sensitive to Slit.

The apparent insensitivity of posterior crista afferents to Slits might be explained if the Slits are unable to overcome the attractive influence of secreted ligands emanating from the target, such as BMPs and FGFs that were previously shown to promote SAG neurite outgrowth *in vitro* (Fantetti and Fekete, 2012). Also, we have no evidence that the growth cones of posterior crista afferents present Robo on their surface. Even if Slit receptors are

expressed by these growth cones, this does not always predict how axons will respond to Slits. Different isoforms of the Robo receptor can be responsible for differential responses to Slit in the *Drosophila* nervous system (Evans and Bashaw, 2010). It is possible that a Robo-independent mechanism could underlie responsiveness to Slits in the inner ear, given that an unidentified Slit receptor has been posited in the spinal cord (Jaworski et al., 2010).

4.3 Lack of responsiveness to Slits *in vitro*

One strategy to evaluate neuronal responsiveness to particular axon guidance molecules is to test them in isolation, so as to minimize the presence of redundant or conflicting signals. Because Slits function as repellents, we used culture conditions that promoted good survival and robust axon outgrowth from SAG explants and were thus appropriate to detect repulsion. These conditions were sufficient to reveal a strong repulsive action of Semaphorin3E on SAG neurons, despite the presence of NT3 and CNTF as survival factors (Fantetti et al., 2011). As a parallel to that study, here we sought to evaluate neurite outgrowth when cultured SAG explants were confronted with excess Slit proteins in the absence of target tissue. This assay will simultaneously test all SAG populations, including both auditory and vesitibular neurons, which are not readily distinguished in explants. Furthermore, the assay cannot differentiate between the central and peripheral processes of the bipolar SAG neurons.

When SAG explants were taken from HH20-25 embryos, there was no significant difference in neurite outgrowth related to the presence or absence of Slits. Not only was the average neurite length similar between control and Slit-treated groups, but the outgrowth density was also comparable. Slits are also known to have effects on branching (Sang et al., 2002). If there were differences in neurite complexity or other features, some of those may have been revealed quantitatively by the pixel measurements. We did not observe enhanced bundling or other obvious changes in neurite morphology for SAGs grown in the presence of purified Slits. However, we cannot rule out the possibility that an enhancement in neurite complexity or branching was present, but was exactly balanced by a decrease in cell survival in treated explants. We conclude that the majority of otic neurites do not respond to Slit1 or Slit2 as a chemorepellant *in vitro*, at least at the stages tested.

4.4 Heterogeneity in responsiveness to Slits

There are several ways to reconcile the negative data obtained from *in vitro* assays with the positive data generated by *in vivo* electroporation into the anterior crista. First, if anterior crista afferents are the only subpopulation responsive to Slits at the stages tested *in vitro*, they may be too few to detect when the entire SAG is explanted and assayed. Second, axonal heterogeneity extends beyond differences in target projections (both central and peripheral) to include asynchrony in neuronal birthdates and the timing of pathfinding. Slit responsiveness for any individual neuron might also be transient. Neuroblast delamination occurs over an extended time period in the chicken otocyst, beginning on HH14 (Hemond and Morest, 1991) and continuing as late as HH27 (Stone et al., 2003). Likewise, the specification of different sensory organs extends across several days of development (Wu and Oh, 1996). Thus, neurite responsiveness to Slits may be transient and dependent on the age of the neuron since its final mitotic division, and/or on the age when its target organ arises. If so, SAG neurons explanted at a particular stage may not respond synchronously and homogenously. Finally, the lack of an effect on neurite outgrowth *in vitro* may be due to the culture conditions used. For example, it is possible that the Slit proteins require some additional factors to modify SAG neurite outgrowth and that these factors are absent *in vitro*, but are present *in vivo*. Also, the presence of non-neuronal cells in the cultures may have indirectly influenced neuronal outgrowth and/or Slit responsiveness. Schwann cells express neurite-promoting neurotrophic factors and can modify spiral ganglion neurite outgrowth *in*

vitro (Hansen et al., 2001; Bostrom et al., 2009; Whitlon et al., 2009; Jeon et al., 2011). In summary, SAG neurons are heterogeneous in their responsiveness to Slits, possibly due to the timing of their development, intrinsic differences in their preferred target (such as the anterior crista), or the *in vitro* culture conditions.

5 Conclusions

We conclude that while many otic axons are unresponsive to Slits, at least one subset, namely those projecting to the anterior crista, can be repelled by either Slit1 or Slit2. This study provides evidence that some otic afferents may use Slit1 and/or Slit2 as a guidance cue while they are pathfinding to their peripheral sensory targets in the ear.

Acknowledgments

This work was funded by the National Institutes of Health Grant RO1DC002756 and the Purdue Research Foundation. We are grateful to Dr. Bruce Craig (Purdue University) for expert statistical consultation and analysis. We thank Doris Wu for advice with experiments and Deb Biesemeier and Christine Dee for assistance with histology. The pEFX-GFP and pEFX plasmids were provided by Dr. Cliff Ragsdale (University of Chicago), while the CMV-hSlit plasmids were provided by Dr. William Andrews (University College London). The 9E10 myc (developed by J.M. Bishop) and 3A10 (developed by T.M. Jessell and collaborators) antibodies were obtained from the Developmental Studies Hybridoma Bank developed under the auspices of the NICHD and maintained by The University of Iowa, Department of Biology, Iowa City, IA 52242.

References

Adamska M, Herbrand H, Adamski M, Kruger M, Braun T, Bober E. FGFs control the patterning of the inner ear but are not able to induce the full ear program. Mech Dev. 2001; 109:303–313. [PubMed: 11731242]

Agarwala S, Sanders TA, Ragsdale CW. Sonic hedgehog control of size and shape in midbrain pattern formation. Science. 2001; 291:2147–2150. [PubMed: 11251119]

Appler JM, Goodrich LV. Connecting the ear to the brain: Molecular mechanisms of auditory circuit assembly. Prog Neurobiol. 2011; 93:488–508. [PubMed: 21232575]

Bank LM, Bianchi LM, Ebisu F, Lerman-Sinkoff D, Smiley EC, Shen YC, Ramamurthy P, Thompson DL, Roth TM, Beck CR, et al. Macrophage migration inhibitory factor acts as a neurotrophin in the developing inner ear. Development. 2012; 139:4666–74. [PubMed: 23172918]

Bashaw GJ, Goodman CS. Chimeric axon guidance receptors: the cytoplasmic domains of slit and netrin receptors specify attraction versus repulsion. Cell. 1999; 97:917–926. [PubMed: 10399919]

Battisti AC, Fekete DM. Slits and robos in the developing chicken inner ear. Dev Dyn. 2008; 237:476–484. [PubMed: 18213576]

Bell D, Streit A, Gorospe I, Varela-Nieto I, Alsina B, Giraldez F. Spatial and temporal segregation of auditory and vestibular neurons in the otic placode. Dev Biol. 2008; 322:109–120. [PubMed: 18674529]

Bianchi LM, Cohan CS. Effects of the neurotrophins and CNTF on developing statoacoustic neurons: comparison with an otocyst-derived factor. Dev Biol. 1993; 159:353–65. [PubMed: 8365572]

Bianchi LM, Gray NA. EphB receptors influence growth of ephrin-B1-positive statoacoustic nerve fibers. European Journal of Neuroscience. 2002; 16:1499–1506. [PubMed: 12405963]

Bianchi LM, Daruwalla Z, Roth TM, Attia NP, Lukacs NW, Richards AL, White IO, Allen SJ, Barald KF. Immortalized mouse inner ear cell lines demonstrate a role for chemokines in promoting the growth of developing statoacoustic ganglion neurons. J Assoc Res Otolaryngol. 2005; 6:355–67. [PubMed: 16240240]

Bostrom M, Khalifa S, Bostrom H, Liu W, Friberg U, Rask-Andersen H. Effects of neurotrophic factors on growth and glial cell alignment of cultured adult spiral ganglion cells. Audiol Neurootol. 2009; 15:175–186. [PubMed: 19851064]

Brors D, Bodmer D, Pak K, Aletsee C, Schafers M, Dazert S, Ryan AF. EphA4 provides repulsive signals to developing cochlear ganglion neurites mediated through ephrin-B2 and -B3. J Comp Neurol. 2003; 462:90–100. [PubMed: 12761826]

Camarero G, Leon Y, Gorospe I, De Pablo F, Alsina B, Giraldez F, Varela-Nieto I. Insulin-like growth factor 1 is required for survival of transit-amplifying neuroblasts and differentiation of otic neurons. Dev Biol. 2003; 262:242–253. [PubMed: 14550788]

Chang W, Lin Z, Kulessa H, Hebert J, Hogan BL, Wu DK. Bmp4 is essential for the formation of the vestibular apparatus that detects angular head movements. PLoS Genet. 2008; 11:e1000050. [PubMed: 18404215]

Chilton JK, Guthrie S. Cranial expression of class 3 secreted semaphorins and their neuropilin receptors. Dev Dyn. 2003; 228:726–733. [PubMed: 14648849]

Cole LK, Le Roux I, Nunes F, Laufer E, Lewis J, Wu DK. Sensory organ generation in the chicken inner ear: contributions of bone morphogenetic protein 4, serrate1, and lunatic fringe. J Comp Neurol. 2000; 424:509–520. [PubMed: 10906716]

Coate TM, Kelly MW. Making connections in the inner ear: recent insights into the development of spiral ganglion neurons and their connectivity with sensory hair cells. Semin Cell Dev Biol. 2013; 24:460–469. [PubMed: 23660234]

Coate TM, Raft S, Zhao X, Ryan AK, Crenshaw EB 3rd, Kelley MW. Otic mesenchyme cells regulate spiral ganglion axon fasciculation through a Pou3f4/EphA4 signaling pathway. Neuron. 2012; 73:49–63. [PubMed: 22243746]

D'Amico-Martel A. Temporal patterns of neurogenesis in avian cranial sensory and autonomic ganglia. American Journal of Anatomy. 1982; 163:351–372. [PubMed: 7091019]

Dalby B, Cates S, Harris A, Ohki EC, Tilkins ML, Price PJ, Ciccarone VC. Advanced transfection with Lipofectamine 2000 reagent: primary neurons, siRNA, and high-throughput applications. Methods. 2004; 33:95–103. [PubMed: 15121163]

Dickson BJ, Gilestro GF. Regulation of commissural axon pathfinding by slit and its Robo receptors. Annu Rev Cell Dev Biol. 2006; 22:651–675. [PubMed: 17029581]

Evans TA, Bashaw GJ. Functional diversity of Robo receptor immunoglobulin domains promotes distinct axon guidance decisions. Curr Biol. 2010; 20:567–572. [PubMed: 20206526]

Fantetti KN, Fekete DM. Members of the BMP, Shh and FGF morphogen families promote chicken statoacoustic ganglion neurite outgrowth and neuron survival in vitro. Dev Neurobiol. 2012; 72:1213–1228. [PubMed: 22006861]

Fantetti KN, Fekete DM. Dissection and culture of chick statoacoustic ganglion and spinal cord explants in collagen gels for neurite outgrowth assays. J Vis Exp. 2011; 58:e3600.10.3791/3600

Fantetti KN, Zou Y, Fekete DM. Wnts and Wnt inhibitors do not influence axon outgrowth from chicken statoacoustic ganglion neurons. Hear Res. 2011; 278:86–95. [PubMed: 21530628]

Fekete DM, Campero AM. Axon guidance in the inner ear. Int J Dev Biol. 2007; 51:549–556. [PubMed: 17891716]

Fritzsch B, Pauley S, Matei V, Katz DM, Xiang M, Tessarollo L. Mutant mice reveal the molecular and cellular basis for specific sensory connections to inner ear epithelia and primary nuclei of the brain. Hear Res. 2005; 206:52–63. [PubMed: 16080998]

Ginzberg RD, Gilula NB. Synaptogenesis in the vestibular sensory epithelium of the chick embryo. J Neurocytol. 1980; 9:405–424. [PubMed: 6969297]

Gu C, Rodriguez ER, Reimert DV, Shu T, Fritzsch B, Richards LJ, Kolodkin AL, Ginty DD. Neuropilin-1 conveys semaphorin and VEGF signaling during neural and cardiovascular development. Dev Cell. 2003; 5:45–57. [PubMed: 12852851]

Hamburger V, Hamilton HL. A series of normal stages in the development of the chick embryo. J of Morphol. 1951; 88:49–91. [PubMed: 24539719]

Hammond R, Vivancos V, Naeem A, Chilton J, Mambetisaeva E, Andrews W, Sundaresan V, Guthrie S. Slit-mediated repulsion is a key regulator of motor axon pathfinding in the hindbrain. Development. 2005; 132:4483–4495. [PubMed: 16162649]

Hansen MR, Zha XM, Bok J, Green SH. Multiple distinct signaling pathways, including an autocrine neurotrophic mechanism, contribute to the survival-promoting effect of depolarization on spiral ganglion neurons in vitro. J Neurosci. 2001; 21:2256–2267. [PubMed: 11264301]

Hemond SG, Morest DK. Ganglion formation from the otic placode and the otic crest in the chick embryo: mitosis, migration, and the basal lamina. Anat Embryol (Berl). 1991; 184:1–13. [PubMed: 1928740]

Holmes G, Niswander L. Expression of slit-2 and slit-3 during chick development. Dev Dyn. 2001; 222:301–307. [PubMed: 11668607]

Hossain WA, D'Sa C, Morest DK. Interactive roles of fibroblast growth factor 2 and neurotrophin 3 in the sequence of migration, process outgrowth, and axonal differentiation of mouse cochlear ganglion cells. J Neurosci Res. 2008; 86:2376–2391. [PubMed: 18438927]

Hossain WA, Morest DK. Fibroblast growth factors (FGF-1, FGF-2) promote migration and neurite growth of mouse cochlear ganglion cells in vitro: immunohistochemistry and antibody perturbation. Journal of Neuroscience Research. 2000; 62:40–55. [PubMed: 11002286]

Hossain WA, Zhou X, Rutledge A, Baier C, Morest DK. Basic fibroblast growth factor affects neuronal migration and differentiation in normotypic cell cultures from the cochleovestibular ganglion of the chick embryo. Experimental Neurology. 1996; 138:121–143. [PubMed: 8593888]

Jaworski A, Long H, Tessier-Lavigne M. Collaborative and specialized functions of Robo1 and Robo2 in spinal commissural axon guidance. J Neurosci. 2010; 30:9445–9453. [PubMed: 20631173]

Jeon EJ, Xu N, Xu L, Hansen MR. Influence of central glia on spiral ganglion neuron neurite growth. Neuroscience. 2011; 177:321–334. [PubMed: 21241783]

Kennedy TE, Serafini T, de la Torre JR, Tessier-Lavigne M. Netrins are diffusible chemotropic factors for commissural axons in the embryonic spinal cord. Cell. 1994; 78:425–435. [PubMed: 8062385]

Krull CE. A primer on using in ovo electroporation to analyze gene function. Dev Dyn. 2004; 229:433–439. [PubMed: 14991698]

Kuratani S, Tanaka S, Ishikawa Y, Zukeran C. Early development of the facial nerve in the chick embryo with special reference to the development of the chorda tympani. Am J Anat. 1988; 182:169–182. [PubMed: 2456687]

Li HS, Chen JH, Wu W, Fagaly T, Zhou L, Yuan W, Dupuis S, Jiang ZH, Nash W, Gick C, Ornitz DM, Wu JY, Rao Y. Vertebrate slit, a secreted ligand for the transmembrane protein roundabout, is a repellent for olfactory bulb axons. Cell. 1999; 96:807–818. [PubMed: 10102269]

Momose T, Tonegawa A, Takeuchi J, Ogawa H, Umesono K, Yasuda K. Efficient targeting of gene expression in chick embryos by microelectroporation. Dev Growth Differ. 1999; 41:335–344. [PubMed: 10400395]

Patel K, Nash JA, Itoh A, Liu Z, Sundaresan V, Pini A. Slit proteins are not dominant chemorepellents for olfactory tract and spinal motor axons. Development. 2001; 128:5031–5037. [PubMed: 11748139]

Pauley, S.; Matei, V.; Beisel, K.; Fritzsch, B. Wiring the ear to the brain: the molecular basis of neurosensory development, differentiation, and survival. In: Kelley, MW.; Wu, DK.; Popper, AN.; Fay, RR., editors. Development of the Inner Ear. New York, NY: Spring; 2005. p. 85-121.

Reeber SL, Kaprielian Z. Leaving the midline: how Robo receptors regulate the guidance of post-crossing spinal commissural axons. Cell Adh Migr. 2009; 3:300–304. [PubMed: 19556886]

Rubel EW, Fritzsch B. Auditory system development: primary auditory neurons and their targets. Annu Rev Neurosci. 2002; 25:51–101. [PubMed: 12052904]

Sang Q, Wu J, Rao Y, Hsueh YP, Tan SS. Slit promotes branching and elongation of neurites of interneurons but not projection neurons from the developing telencephalon. Mol Cell Neurosci. 2002; 21:250–265. [PubMed: 12401446]

Siddiqui SA, Cramer KS. Differential expression of Eph receptors and ephrins in the cochlear ganglion and eighth cranial nerve of the chick embryo. J Comp Neurol. 2005; 482:309–319. [PubMed: 15669077]

Tessarollo L, Coppola V, Fritzsch B. NT-3 replacement with brain-derived neurotrophic factor redirects vestibular nerve fibers to the cochlea. J Neurosci. 2004; 24:2575–2584. [PubMed: 15014133]

Vargesson N, Luria V, Messina I, Erskine L, Laufer E. Expression patterns of Slit and Robo family members during vertebrate limb development. Mech Dev. 2001; 106:175–180. [PubMed: 11472852]

Von Bartheld CS, Patterson SL, Heuer JG, Wheeler EF, Bothwell M, Rubel EW. Expression of nerve growth factor (NGF) receptors in the developing inner ear of chick and rat. Development. 1991; 113:455–470. [PubMed: 1664321]

Wang SZ, Ibrahim LA, Kim YJ, Gibson DA, Leung HC, Yuan W, Zhang KK, Tao HW, Ma L, Zhang LI. Slit/Robo Signaling Mediates Spatial Positioning of Spiral Ganglion Neurons during Development of Cochlear Innervation. J Neurosci. 2013; 30:12242–12254. [PubMed: 23884932]

Webber A, Raz Y. Axon guidance cues in auditory development. Anat Rec A Discov Mol Cell Evol Biol. 2006; 288:390–396. [PubMed: 16550548]

Whitehead MC, Morest DK. The development of innervation patterns in the avian cochlea. Neuroscience. 1985; 14:255–276. [PubMed: 3974881]

Whitlon DS, Tieu D, Grover M, Reilly B, Coulson MT. Spontaneous association of glial cells with regrowing neurites in mixed cultures of dissociated spiral ganglia. Neuroscience. 2009; 161:227–235. [PubMed: 19324078]

Wu DK, Oh SH. Sensory organ generation in the chick inner ear. J Neurosci. 1996; 16:6454–6462. [PubMed: 8815924]

Ypsilanti AR, Zagar Y, Chedotal A. Moving away from the midline: new developments for Slit and Robo. Development. 2010; 137:1939–1952. [PubMed: 20501589]

Zhou CQ, Lee J, Henkemeyer MJ, Lee KH. Disruption of ephrin B/Eph B interaction results in abnormal cochlear innervation patterns. Laryngoscope. 2011; 121:1541–7. [PubMed: 21647913]

Abbreviations

CMV	cytomegalovirus
CNTF	Ciliary neurotrophic factor
df	degrees of freedom
E	Embryonic day
EF-1α	elongation factor 1 alpha
GFP	green fluorescent protein
HBSS	Hank’s Balanced Salt Solution
HEK	Human embryonic kidney
HH	Hamburger and Hamilton stage
NF70	Neurofilament 70
NT3	Neurotrophin-3
PBS	Phosphate-buffered saline
Robo	Roundabout
SAG	Statoacoustic ganglion

Highlights

- The majority of chick SAG neurites are unresponsive to Slits when presented *in vitro*
- Chick olfactory bulb explants confirm bioactivity of the tested molecules
- Slit misexpression within the anterior crista reduces innervation *in vivo*
- Posterior crista afferents are unresponsive to Slits *in vivo*
- Prosensory formation and gangliogenesis are unaffected in Slit-electroporated ears

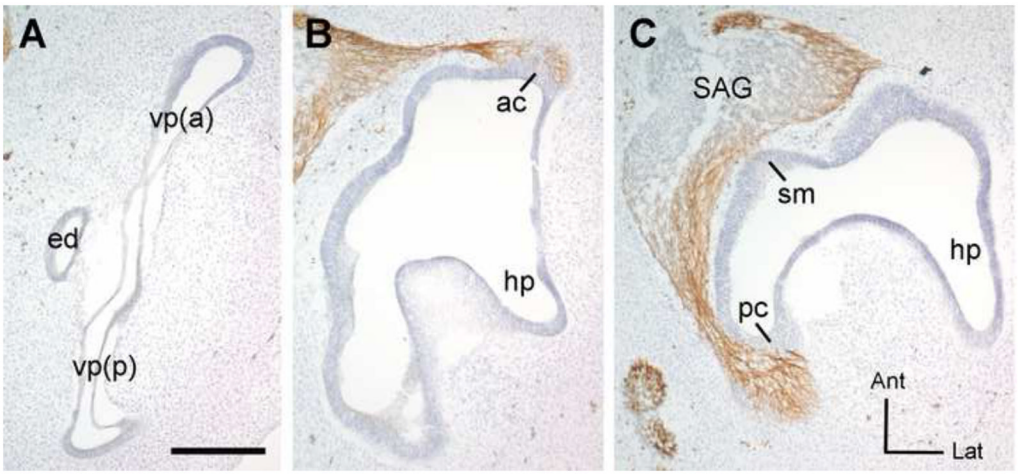

Figure 1. Horizontal histological sections show the plane of section used to evaluate canal morphogenesis and cristae innervation patterns

Frozen sections were immunostained with 3A10 antibody to detect the axons (brown) and counterstained with cresyl violet to visualize the otic epithelium. This is the untransfected (left) ear from an experimental embryo processed at HH28 3 days following electroporation into the contralateral ear. Images were reversed to match the orientation of specimens shown in Figures 2-4. This exemplar corresponds to the survival times of the embryo shown in figure 4. The embryos shown in Figures 2 and 3 were processed one day earlier, at 2-days post-electrorporation. These sections are arranged from dorsal to ventral (A-C). In panel (A), a morphologically normal vertical canal pouch is elongated along the anterior-posterior axis, flattened in the medial-lateral dimension as the walls of the pouch approach each other in advance of fusion, and has slight dilation of the rims of the pouch where the future canals will be. Panel B is a more ventral section, through the plane of axons projecting into the anterior crista primordium. Panel C is even more ventral to panel B. In this plane, some axons leave the statoacoustic ganglion (SAG) and immediately enter the primordium of the saccular macula. Others project well past this location to enter the posterior crista primordium. Abbreviations: ac, anterior crista; Ant, anterior; vp(a), vertical pouch, anterior part (will become the anterior semicircular canal); ed, endolymphatic duct; hp, horizontal pouch (will become the lateral semicircular canal); Lat, lateral; pc, posterior crista; vp(p), vertical pouch, posterior part (will become the posterior semicircular canal); SAG, statoacoustic ganglion; sm, saccular macula; pc, posterior crista. Scale bar = 200 microns.

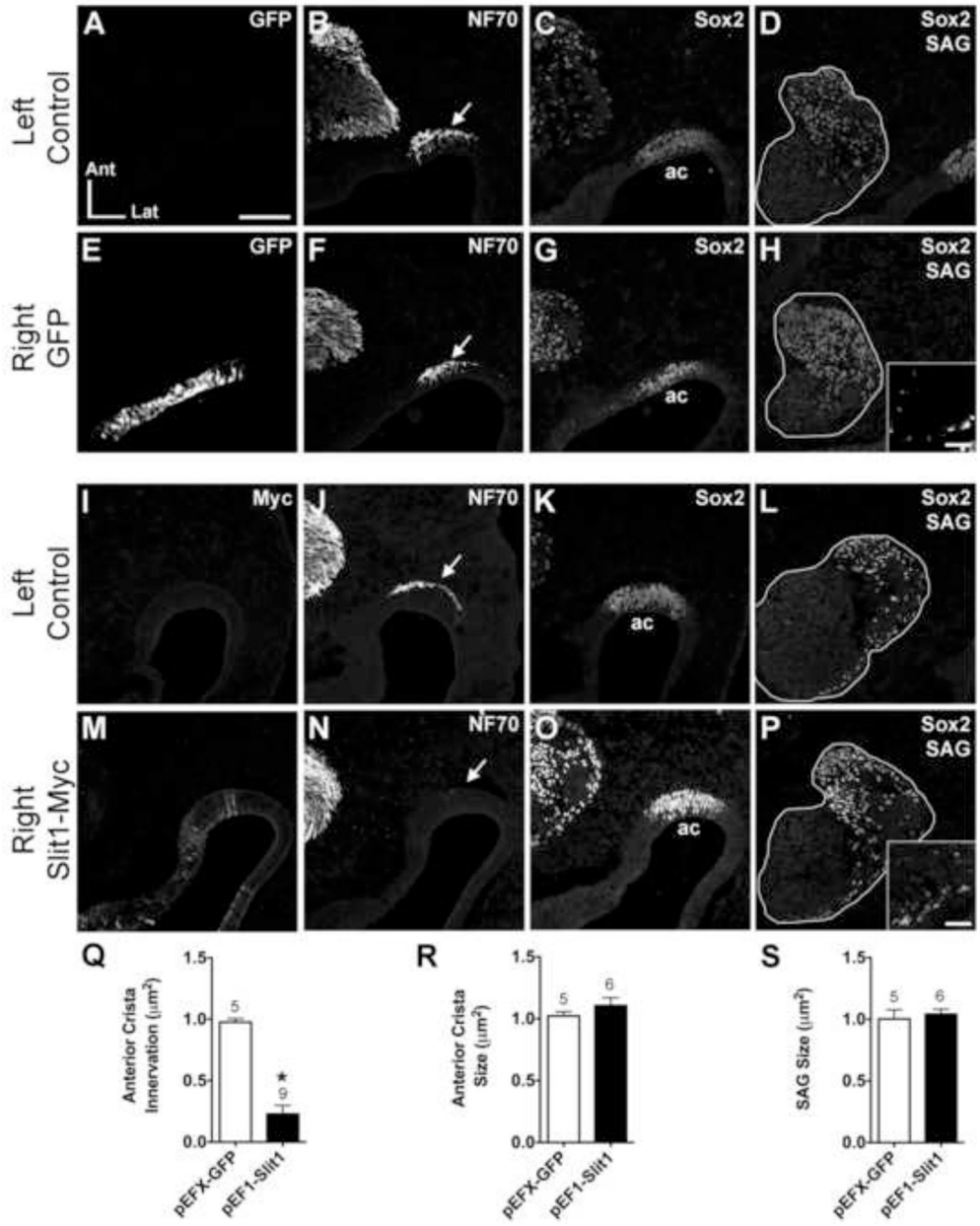

Figure 2. Anterior crista afferents are repelled from the anterior crista following pEF1-hSlit1 electroporation

Serial horizontal sections through the left (unelectroporated) or right (electroporated) otocysts of embryos transfected with either pEFX-GFP (HH23; A-H) or pEF1-Slit1 (HH26; I-P). In these and subsequent figures, images of the left and right ear are from the same embryo, but the one side was mirror-image reversed to facilitate comparisons to the other side. Sections were immunostained with antibodies indicated in the upper right of each panel to label transfected cells (myc), axons (NF70) and prosensory domains (Sox2). Arrows indicate axon bundles adjacent to the anterior crista (ac) primordia. pEF1-Slit1 electroporation resulted in diffuse expression of Slit1-myc in the anterior crista primordium (M). The anterior crista of the Slit-electroporated ear (N) lacks afferent innervation as compared to the control ear of the same embryo (J). Sox2 marks the anterior crista primordium in each ear (C, G, K, O). The size and position of the SAGs (outlined in white)

are similar across treatment groups (D, H, L, P). Insets in H and P show GFP- and Myc-immunolabeled cells in the SAGs, respectively. Quantification of anterior crista innervation (Q), anterior crista size (R), and SAG size (S). *$p<0.0001$ statistically significant from unelectroporated controls. The number above the bars represents the number of ears analyzed in each treatment group. Abbrevations: Ant, anterior; ac, anterior crista; Lat, lateral; SAG, statoacoustic ganglion. Scale bar in Panel A = 100 μm for all large panels. Scale bar for insets in Panel H = 25 μm.

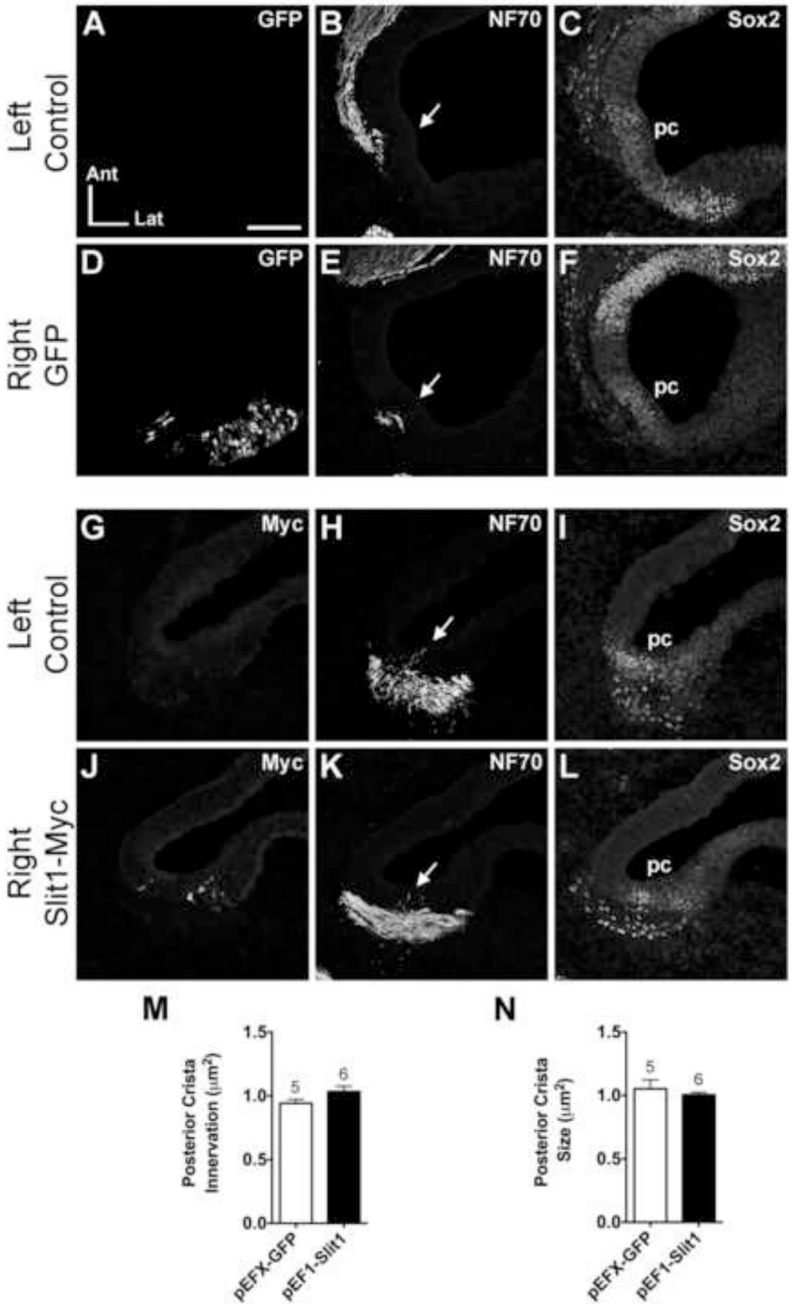

Figure 3. Normal posterior crista innervation following pEF1-Slit1 electroporation

Serial horizontal sections through the left and right posterior cristae of pEFX-GFP (HH24; A-F) and pEF1-Slit1 (HH26; G-L) electroporated embryos. Arrows indicate projections into the posterior crista primordium. Innervation of the Slit1-electroporated posterior crista (K) resembles the control ear (H). Sox2 labels the posterior crista in each ear (C, F, I, L). Quantification of posterior crista innervation (M) and size (N). See legend of Figure 2 for labeling conventions. Abbreviations: Ant, anterior; Lat, lateral; pc, posterior crista; SAG, statoacoustic ganglion. Scale bar = 100 μm.

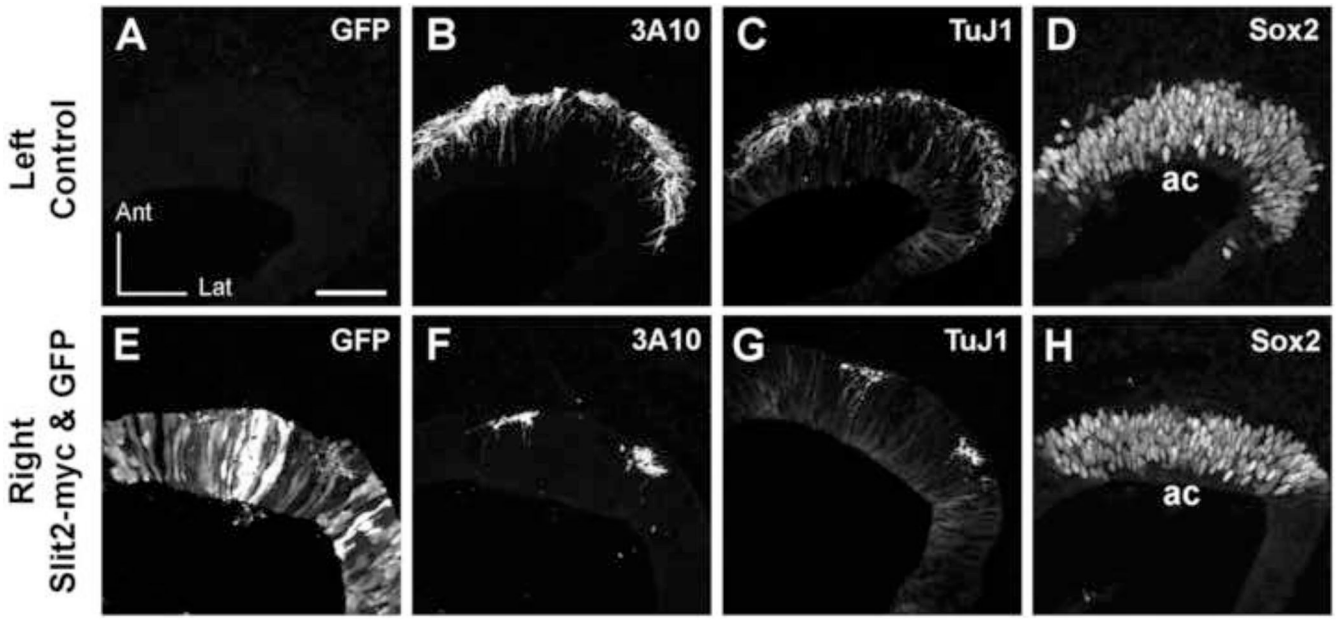

Figure 4. Anterior crista afferents are reduced 3 days after co-electroporation of pEF1-Slit2 and pEFX-GFP in their target domain

Serial horizontal sections through the left or right otocysts of an embryo in which both pEFX-GFP and pEF1-Slit2 were co-electroporated into the right ear. The same sections are shown in alternate color channels for panels A/B and C/D, while the remaining panels are from sequential sections through each ear. Images of the right ear were mirror-image reversed to facilitate comparing to the left ear. The antibodies used are indicated in the upper right of each panel. GFP is undetectable in the left ear (A) but is present in a subset of cells distributed throughout the anterior pole of the right ear (E). Robust innervation of the anterior crista primordium of the left ear (B, C) can be contrasted with the paucity of axons detected beneath and within the anterior crista of the right ear (F,G). In the right ear, two axon bundles flank an area of particularly strong GFP expression in the epithelium that is completely devoid of axonal projections. Sox2 labeling reveals the anterior crista primordium on each side (D,H). Abbrevations: ac, anterior crista; Ant, anterior; Lat, lateral. Scale bar = 50 μm.

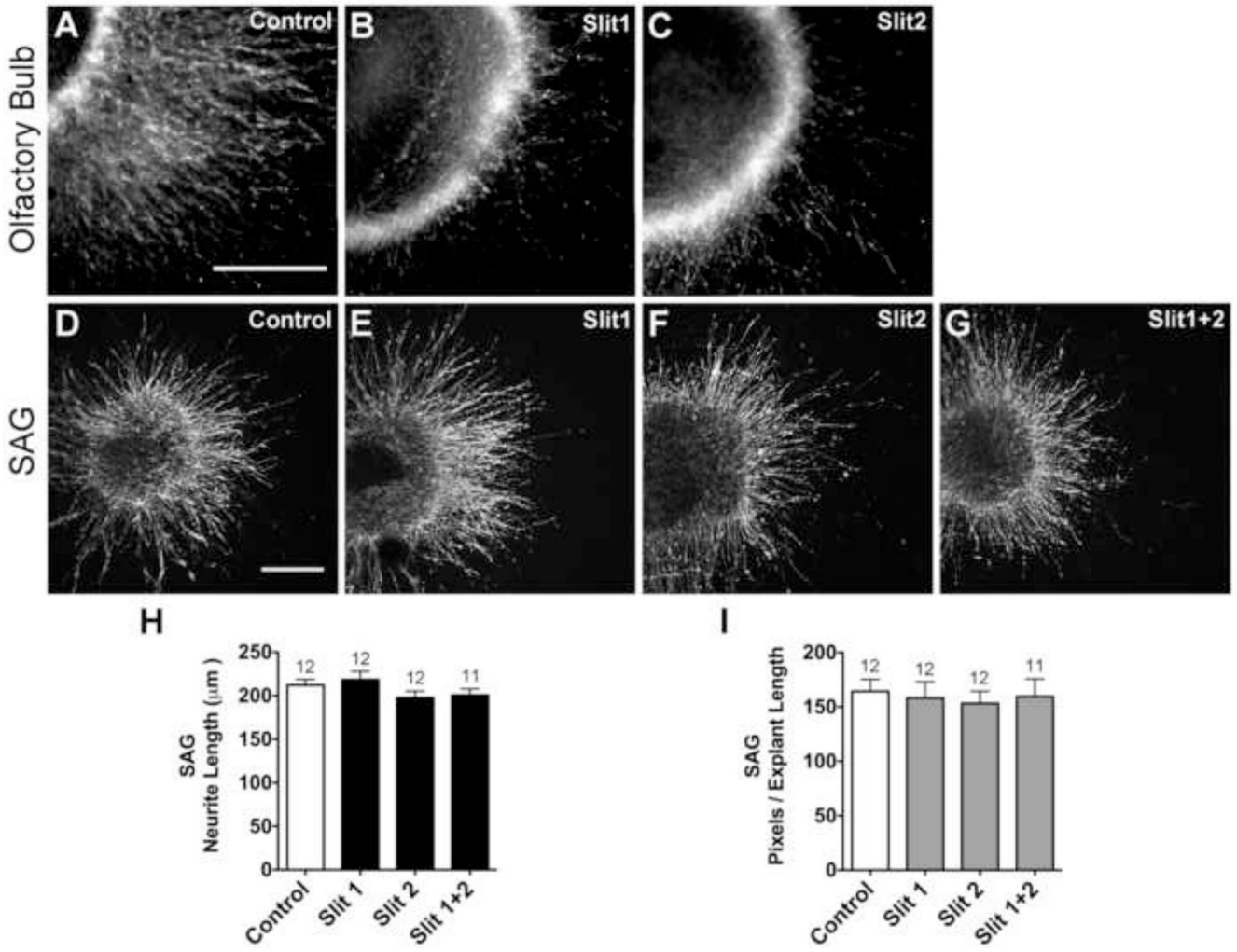

Figure 5. Purified Slit1 and Slit2 proteins inhibit HH33-34 chick olfactory bulb neurite outgrowth but do not affect HH20-25 SAG neurite outgrowth

Olfactory bulb explants cultured for 24 hours with either 20 μg/ml mouse Slit1 (B) or 20 μg/ml mouse Slit2 (C) display reduced neurite outgrowth compared to explants cultured without Slit (Control; A), confirming that the mouse Slit proteins are bioactive under these culture conditions. SAG explants display similar neurite outgrowth patterns when cultured for 40 hours without (D) or with Slit1 (E), Slit2 (F) or Slit1+2 (G). Quantification of SAG neurite length (H) and pixel number (I). Bars represent the mean for each treatment group (±SE). The number of explants analyzed, for each treatment group, is above the bars. Pixel data partially overlap with samples used for length measurements. Scale bars = 200 μm.

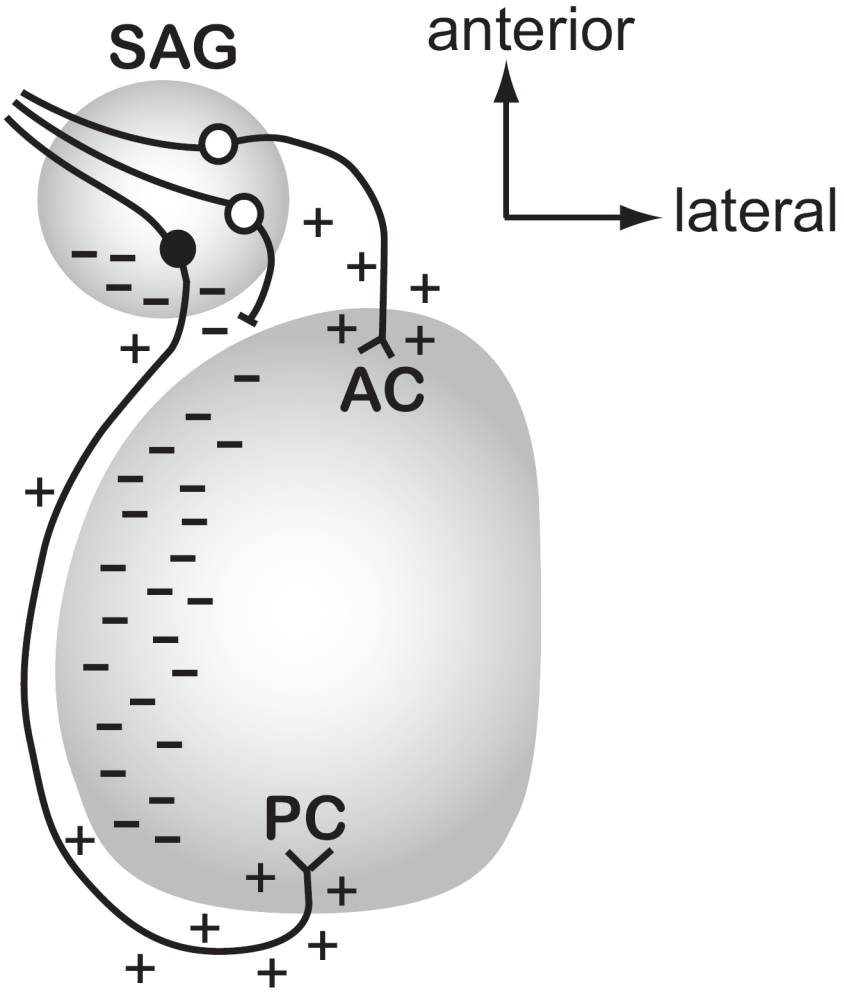

Figure 6. Model for how Slit activity may direct afferent outgrowth into the otocyst *in vivo*

This figure predicts where Slit1 and/or Slit2 proteins (indicated as dashes) are localized in the normal ear at the time when afferents to the anterior and posterior crista are projecting from the SAG towards their targets (approximately HH17-22). This model takes into account the experimental observation that afferents projecting to the anterior vs. posterior cristae demonstrate differential responsiveness to Slits as a mechanism by which these two populations of axons are directed to grow in opposite directions. We predict that the diffusion of Slit proteins (indicated by dashes) from the posterior SAG and medial otic vesicle will repel anterior crista afferents (white cell bodies) from initiating trajectories in the posterior direction. If they do project posteriorly, they would be prevented from advancing (shown as an axon with a blocked process) and may then be redirected anteriorly to reach their target. In contrast, a neuron seeking to innervate the posterior crista (black cell body) is insensitive to the same Slit cues, allowing it to pass through or alongside territories that have an abundance of Slit proteins. The model also depicts putative attractive cues (shown as + symbols) along the pathways or emanating from the targets, although additional unknown repulsive cues (not shown) may also confine axonal trajectories to specific pathways. Abbreviations: AC, anterior crista; PC, posterior crista; SAG, statoacoustic ganglion.

Table 1

Innervation of the anterior or posterior cristae 2-3 days after electroporation of plasmids on embryonic day 3 successfully targeted the prosensory domain.

Organ targeted Plasmid	Number of ears with Normal Innervation	Number of ears with Reduced Innervation
Anterior Crista		
pEFX-GFP	23	3
pEF1-Slit1-myc	4	18
pEF1-Slit2-myc & pEFX-GFP	1	6
Posterior Crista		
pEFX-GFP	16	0
pEF1-Slit1-myc	20	0
pEF1-Slit2-myc & pEFX-GFP	6	0